ORIGINAL SCIENTIFIC PAPER

CROATICA CHEMICA ACTA

Croat. Chem. Acta **2018**, *91*(2)
Published online: July 3, 2018
DOI: 10.5562/cca3362

HKD 1926

Order-Disorder in Diaquobis(salicylato)copper(II) Revisited

Martin Lutz, Loes M. J. Kroon-Batenburg*

Crystal and Structural Chemistry, Bijvoet Center for Biomolecular Research, Utrecht University, Padualaan 8, 3584 CH Utrecht, The Netherlands
* Corresponding author's e-mail address: l.m.j.kroon-batenburg@uu.nl

RECEIVED: May 4, 2018 ⋆ REVISED: June 21, 2018 ⋆ ACCEPTED: June 28, 2018

THIS PAPER IS DEDICATED TO DR. BISERKA KOJIĆ-PRODIĆ ON THE OCCASION OF HER 80TH BIRTHDAY

Abstract: We re-investigated the crystal structure of diaquobis(salicylato)copper(II), CuSal, which is an OD material with disordered layer stacking. The diffraction pattern consists of sharp Bragg spots and diffuse streaks.
From the Bragg reflections we determined the ordered part of the structure, which can either be described by an orthorhombic or a twinned monoclinic lattice. The main motif of the structure consists of one-dimensional coordination polymers that are connected by hydrogen bonds into two-dimensional layers.
The layer stacking is disordered and from simulations with a Markovian growth models we could fully explain the diffuse streaks of the current structure when the layers are stacked randomly.

Keywords: diffuse scattering, OD structure, hydrogen-bonded layers, copper complex.

INTRODUCTION

THE disorder in the crystal structure of the title compound diaquobis(salicylato)copper(II) (CuSal) has been recognized first by Dornberger-Schiff & Malinowski.[1] In a series of publications this structure has later been investigated in detail by Jagner *et al.* on the basis of the Order-Disorder Theory (OD theory).[2–5] The diffraction pattern is characterized by sharp Bragg reflections for *h* = *even* and diffuse streaks for *h* = *odd*. The diffuse streaks are running in the **c*** direction. According to Jagner *et al.*,[2] the sharp reflections can be indexed either by an orthorhombic or a monoclinic unit cell. These correspond to the phases MDO_1 (orthorhombic) and MDO_2 (monoclinic), where MDO stands for Maximum Degree of Order. In terms of the OD theory, the sharp Bragg reflections can be named *family reflections*. On the locations of the diffuse streaks, the orthorhombic and monoclinic reciprocal unit cells are non-overlapping. Jagner *et al.*[2] find explicit intensity maxima on the streaks which would correspond to either of them.

The structure description of Jagner *et al.*[2] is characterized by one-dimensional coordination polymers along the **b** axis, which are present in both the orthorhombic and the monoclinic description. Hydrogen atoms were not determined and their influence on the crystal packing not discussed. In the monoanionic salicylate ligand it is unclear whether the carboxylate or the hydroxyl group remain protonated. In addition there is an ambiguity for the position of the hydroxy group. Jagner *et al.* used a disorder model which has a partial occupancy for the hydroxy group on both *ortho* positions.

By the reaction of sodium salicylate with copper(II) sulfate we obtained the polymeric $[Cu_2(C_7H_4O_3)_2(H_2O)_2] \cdot 2H_2O$ that contains the dianionic salicylate ligand Sal^{2-} and which we published earlier.[6] In the same crystallization batch we also obtained CuSal of the current study which contains the monoanionic ligand $HSal^-$. The two crystal forms can easily be distinguished by their colour. Crystals with the dianionic salicylate are brown,[6] while the crystals of the current study with monoanionic salicylate are green.

In the context of our studies on salicylates we re-determined the structure of CuSal. With the new diffraction data, hydrogen atoms could be determined and the hydrogen bonding scheme can be discussed. While OD theory is an established, thorough and complete theory of

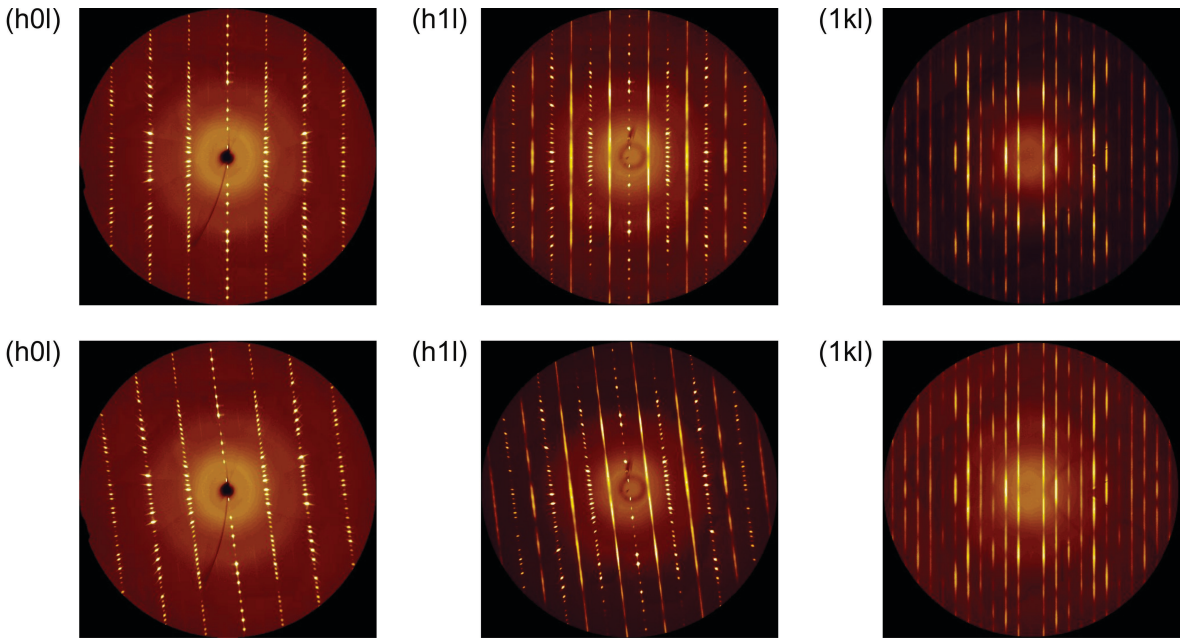

Figure 1. Slices through reciprocal space reconstruction of the data. An orthorhombic (top) and monoclinic (bottom) unit cell were used for their generation with the program `precession` in the Eval15 suite.[10] Diffuse streaks are running in the corresponding **c*** directions and are absent in the zeroth *k* layers.

symmetry [7–9], the symmetry theory does not explain the intensity distribution in the diffraction pattern. We therefore discuss explanations for the diffuse scattering intensities.

RESULTS AND DISCUSSION

Molecular and Crystal Structure

Figure 1 shows two-dimensional reconstructions of the diffraction pattern. The main features are consistent with the observations of Jagner *et al.*[2] and Falch *et al.*[11] The major difference is in the diffuse streaks. The streaks of the current pattern have no explicit intensity maxima whereas Jagner *et al.* could assign maxima to either the orthorhombic or monoclinic unit cell. Consequently, for the refinement of the unit cells and for the evaluation of the X-ray intensities only reflections with *h* = *even* could be used in our case. The data completeness is thus halved. We can choose both lattices for indexing. More experimental details are given below in Table 3 and Table 4. The transformation matrix for the *h* = *even* layers is provided in Equation (1). Slight deviations in the cell parameters of both settings are due to independent data integrations and independent unit cell refinements.

$$\begin{pmatrix} h_{mono} \\ k_{mono} \\ l_{mono} \end{pmatrix} = \begin{pmatrix} 1 & 0 & 0 \\ 0 & 1 & 0 \\ -0.5 & 0 & 1 \end{pmatrix} \begin{pmatrix} h_{ortho} \\ k_{ortho} \\ l_{ortho} \end{pmatrix} \quad (1)$$

Despite the presence of diffuse streaks we set out to determine the atomic structure. Especially interesting is an analysis of the hydrogen bonding situation which has not been discussed by Jagner *et al.*[2]

Orthorhombic Phase MDO_1

Reflections with *h* = *even* can alternatively be indexed with an orthorhombic or monoclinic lattice. In the orthorhombic setting, the asymmetric unit contains two copper atoms, four monoanionic salicylate ligands and four neutral water molecules. In contrast to the literature structure,[2] there is no statistical disorder in the salicylate molecules present. Figure 2 shows a plot of the asymmetric unit. Two of the

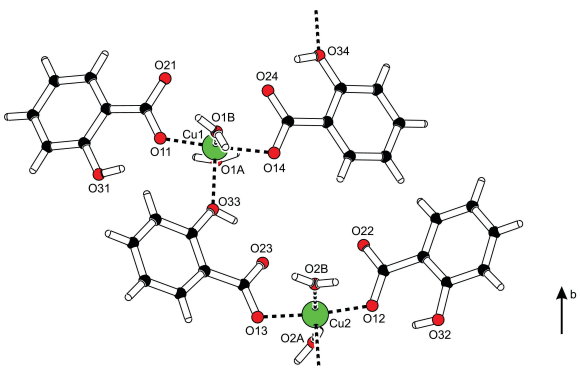

Figure 2. Asymmetric unit of the orthorhombic phase. View approximately along the *a* axis.

Table 1. Hydrogen bonding geometry in the orthorhombic form

D–H···*A*[(a)]	D–H / Å	H···A / Å	D···A / Å	D–H···A / °
O1*A*–H1*A*···O24[i]	0.85	1.91	2.706(10)	155
O1*A*–H1*B*···O21[i]	0.85	1.89	2.676(13)	152
O1*B*–H1*C*···O13[ii]	0.84	1.94	2.766(9)	166
O1*B*–H1*D*···O21[iii]	0.85	1.92	2.766(13)	170
O2*A*–H2*A*···O14[iv]	0.86	1.95	2.762(10)	158
O2*A*–H2*B*···O22[iv]	0.85	2.05	2.713(12)	135
O2*B*–H2*C*···O23[ii]	0.85	1.85	2.634(11)	152
O2*B*–H2*D*···O22[ii]	0.85	1.88	2.620(12)	145
O31–H31···O11	0.84	1.72	2.493(12)	153
O32–H32···O12	0.84	1.92	2.653(9)	145
O33–H33···O23	0.84	1.77	2.513(8)	147
O34–H34···O24	0.84	1.74	2.494(8)	148

[(a)] Symmetry codes: (i) $x-0.5, 1-y, z$; (ii) $x+0.5, -y, z$; (iii) $x+0.5, 1-y, z$; (iv) $x-0.5, -y, z$.

monoanionic salicylate ligands are bridging the copper centers which leads to a one-dimensional polymeric chain in **b** direction. The other two salicylate ligands and the water molecules are non-bridging. All crystallographically independent atoms belong to the same chain.

Monoanionic salicylate complexes are quite common. In the majority of cases, the carboxylate group is deprotonated and the hydroxyl group is protonated.[12] This situation is also found here for all four independent salicylate ligands. The hydroxyl groups are only involved in intramolecular hydrogen bonds with the carboxylate oxygen of the same salicylate as acceptor. In the terminal salicylates, the metal-coordinated oxygen is the acceptor, and in the bridging salicylates it is the non-coordinated oxygen. The water molecules act as donors for intermolecular hydrogen bonds with again the carboxylate oxygens as acceptors. These hydrogen bonds connect the one-dimensional coordination chains into a two-dimensional network parallel to the **ab** plane. An overview of the hydrogen bonded geometries is provided in Table 1. The two-dimensional layers are further stabilized by $\pi\cdots\pi$ interactions between the phenyl rings of the salicylate ligands within the layers. *Ring*···*ring* distances were determined as 3.423(2)–3.508(3) Å.

In accordance with the description of,[2] the environment of both Cu centers is five-coordinated with a square pyramidal geometry as indicated by the τ parameters[13] of 0.10 and 0.06 for Cu1 and Cu2, respectively. It should be noted that both Cu centers have a sixth oxygen in proximity which originates from the carboxylate group of the bridging salicylate. The corresponding distances Cu1···O24 and Cu2···O23 of 2.710(5) and 2.719(6) Å are

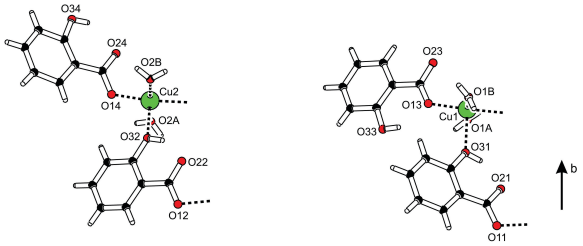

Figure 3. Asymmetric unit of the monoclinic phase. View approximately along –*a*.

quite long. Such long bonds have been observed in octahedral, Jahn-Teller distorted Cu(II) complexes, but the corresponding O-Cu···O angles of 53.5(2) and 53.16(18) ° contradict an octahedral environment and a bonding situation, here. Generally, the coordination mode of asymmetric bonded carboxylate groups is difficult to determine.[14]

The orthorhombic phase has the polar, non-centrosymmetric space group $Pca2_1$. Refinement as an inversion twin results in a Flack parameter[15] of x = 0.50(4) which indicates perfect twinning or centrosymmetry. This value is based on the reflections with h = *even* only.

Monoclinic Phase MDO_2

An alternative indexing of reflections with h = *even* is possible with a monoclinic lattice. We found that quality improved if the intensities are ''de-twinned'' from the orthorhombic contribution (see Experimental Section).

The description in monoclinic symmetry has space group $P2_1/a$. This space group has the same number of symmetry operations as the orthorhombic $Pca2_1$. Consequently, the number of atoms in the asymmetric unit is the same. While in the orthorhombic phase all atoms in the

Table 2. Hydrogen bonding geometry in the monoclinic form

D–H···A[(a)]	D–H / Å	H···A / Å	D···A / Å	D–H···A / °
O1*A*–H1*A*···O21[i]	0.82	1.89	2.637(7)	150
O1*A*–H1*B*···O23[ii]	0.86	1.90	2.636(8)	143
O1*B*–H1*C*···O11[iii]	0.84	1.98	2.789(6)	160
O1*B*–H1*D*···O23[iv]	0.85	1.92	2.758(8)	172
O2*A*–H2*A*···O12[v]	0.86	1.91	2.755(7)	165
O2*A*–H2*B*···O24[ii]	0.85	1.94	2.735(9)	154
O2*B*–H2*C*···O24[iv]	0.88	1.87	2.681(9)	153
O2*B*–H2*D*···O22[vi]	0.86	1.89	2.716(8)	159
O31–H31···O21	0.84	1.76	2.514(5)	149
O32–H32···O22	0.84	1.73	2.476(6)	147
O33–H33···O13	0.84	1.91	2.649(7)	145
O34–H34···O24	0.84	2.11	2.780(8)	136

[(a)] Symmetry codes: (i) $x, y, -z$; (ii) $x-0.5, 0.5-y, z$; (iii) $x+0.5, -y-0.5, z$; (iv) $x+0.5, 0.5-y, z$; (v) $x-0.5, -y-0.5, z$; (vi) $2-x, -y, 1-z$.

asymmetric unit belong to the same coordination chain, in the monoclinic phase they are in two independent chains (Figure 3). Symmetry operations of $Pca2_1$ have become pseudo-operations in $P2_1/a$, and *vice versa*. Again, the hydrogen bonding scheme leads to two-dimensional sheets in the **ab** plane. The hydrogen bonding geometries can be found in Table 2.

The monoclinic lattice can be transformed into a C-centered orthorhombic lattice with doubled volume using the LEPAGE algorithm of the PLATON software.[16] If structure factors are calculated from the monoclinic single-crystal model, the F^2_{calc} have R_{int} = 35 % after transformation to orthorhombic C (NEWSYM routine in PLATON). The orthorhombic symmetry is thus not supported by the atomic model. Still, this orthorhombic geometry needs to be considered as a driving force for possible twinning. In the refinement we included a twin matrix corresponding to a twofold rotation about *hkl* = (0,0,1). This leads to a complete overlap of all reflections (pseudo-orthorhombic twinning) and the twin fraction refined to 0.501(6). The relation between the different unit cells is displayed in Figure 4.

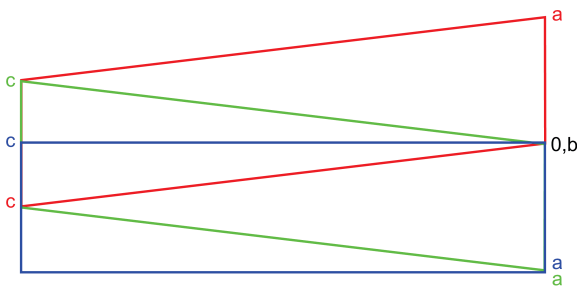

Figure 4. Orientation of the two twinned monoclinic unit cells (red and green) with respect to the orthorhombic unit cell (blue). View along the orthorhombic **b** axis.

The monoclinic unit lattices overlap perfectly with each other. They overlap with the orthorhombic lattice in every second layer. The supercell common to all three unit cells has thus an orthorhombic geometry with the *c* axis doubled. This common supercell is responsible for the sharp Bragg reflections (*family reflections*) in the diffraction pattern.

Structure Comparison

Both the orthorhombic and the monoclinic description of the CuSal structure are characterized by two-dimensional layers in the **ab** plane. These layers are constructed by a coordination chain along **b** which are linked by intermolecular hydrogen bonds and $\pi\cdots\pi$ interactions into two-dimensional layers. A projection along the **a** axis is shown in Figure 5. In this perspective, the two packing arrangements are very similar. The major difference is in the symmetry operations which are indicated by colour schemes in the drawings. In the orthorhombic description all atoms of the asymmetric unit belong to the same coordination chain, while in the monoclinic description they are divided over two symmetry-independent chains.

The stacking difference between the orthorhombic and monoclinic form can be seen in projections along the **b** axis (Figure 6) and the along the **c** axis (Figure 7). The latter is a projection perpendicular to the hydrogen-bonded sheets. The coordination pyramids point upwards along **+b** and downwards along **–b**. The orthorhombic stacking can be converted into the monoclinic one (and *vice versa*) by moving one layer over $\frac{1}{2}$**a**.

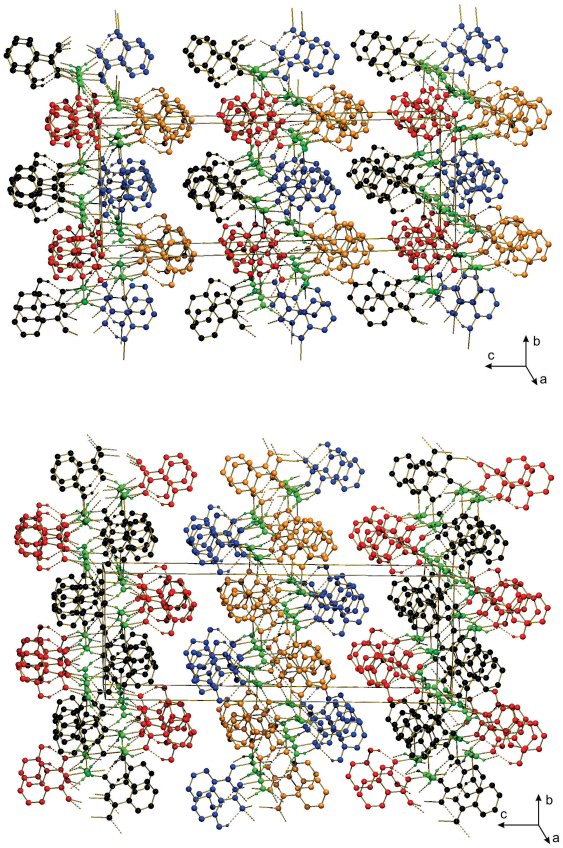

Figure 5. Packing of the hydrogen-bonded layers, viewed approximately along the **a** axis. C–H hydrogen atoms are omitted for clarity. Symmetry-independent salicylate ligands are shown in different colours. The orthorhombic description is shown on top, the monoclinic in the bottom.

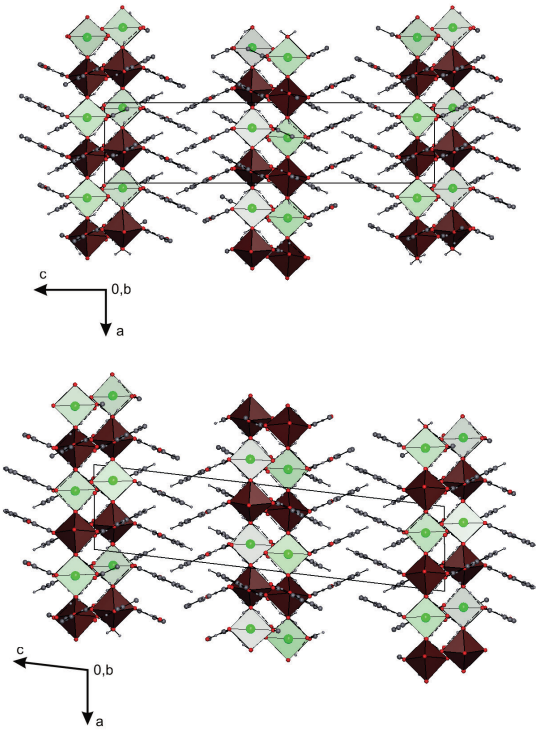

Figure 6. Packing of the hydrogen-bonded layers, viewed along the **b** axis. The orthorhombic description is shown on top, the monoclinic on bottom. CuO_5 coordination units are drawn as square pyramids. Pyramids pointing in the direction of **+b** are shown in brown and pointing along **–b** in green.

For the final results, both structure descriptions have been refined with reflections with *h* = *even* only. This makes structure refinement difficult. Convergence of the refinement is slow and can only be achieved with strong restraints. The obtained atomic displacement parameters and the geometric values for distances and angles remain rather unreliable. Similar difficulties with OD structures are described in the literature.[8] Still, the positions of *ortho* hydroxy groups and of the protonation sites could be reliably determined in the present case. We consider this an important improvement with respect to the earlier descriptions of this structure in the literature.

More information can be obtained from the diffuse streaks with *h* = *odd*. This will be considered in the next section.

Stacking Disorder

The diffusely scattering structure of CuSal can either be described as orthorhombic $Pca2_1$ or monoclinic $P2_1/a$, both with stacking faults along the **c** axis. In either case the structure consists of mirror related pairs of **ab** layers connected by weak van-der-Waals interactions. The stacking fault is a displacement of such a pair over $\frac{1}{2}$**a**, which changes the local packing from orthorhombic to monoclinic, or *vice versa* (Figure 8). A similar one-dimensional disorder has been described for Wollastonite.[17,18] Figure 8 shows the stacking lattice that as such was introduced by Dornberger-Schiff.[19] It has half the size in the **a** direction. On this lattice the structure is completely ordered. Thus reflections with *h* = *even* with respect the original lattice, represent an ordered structure, and can be used to solve the orthorhombic or monoclinic structure. Reflections with *h* = *odd* show the loss of long range order in **c**. In fact reflections (*h* = 2*n* + 1,*k*,*l*) are rods along *l* (Figure 1); these can be interpreted as the Fourier transforms of the arbitrarily stacked **ab** layers. A mathematical description of scattered intensities follows below.

The structure factor of one unit cell is given by:

$$F_A(hkl) = \sum_j f_j e^{2\pi i(hx_j + ky_j + lz_j)} \quad (2)$$

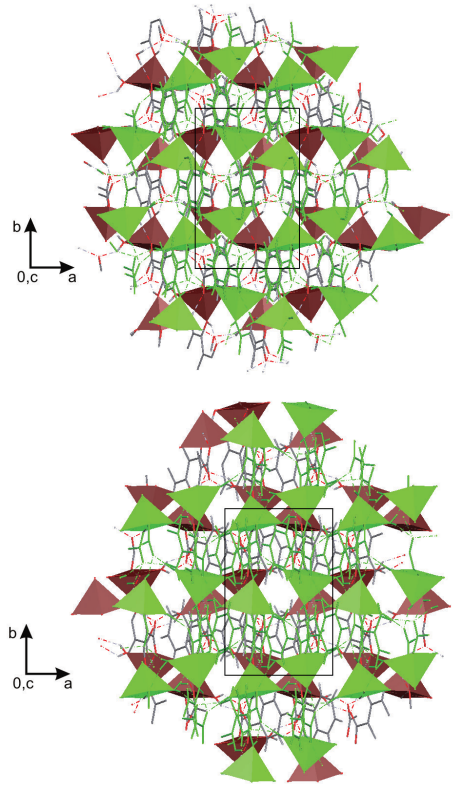

Figure 7. Hydrogen-bonded layers in the **ab** plane, viewed along the **c** axis. CuO_5 coordination units are drawn as square pyramids. Pyramids at height z ≈ 0 are shown in brown, at height z ≈ ½ in green. The orthorhombic description is shown on top, the monoclinic on bottom.

while that of the unit cell displaced over $\frac{1}{2}$**a** is

$$F_B(hkl) = \sum_j f_j e^{2\pi i(h(x_j+\frac{1}{2})+ky_y+lz_j)} = F_A e^{\pi i h} . \quad (3)$$

The structure factor amplitude for the whole crystal is a lattice summation over the $N_1 \times N_2 \times N_3$ unit cells:

$$F_C(hkl) = \sum_{n_1}\sum_{n_2}\sum_{n_3} F_A(hkl) e^{\pi i h p_{n_3}} e^{2\pi i(n_1 h + n_2 k + n_3 l)} \quad (4)$$

where p_{n3} in the phase factor is 0 or 1 for the normal and displaced structure factors, respectively. Since the structure is ordered in **a** and **b** but disordered along **c**, only integer value of *h* and *k* have non-zero contributions, while for *l* also fractional values will contribute and the resulting structure factor is a continuous function in *l*:

$$F_C(hkl) = N_1 N_2 \sum_{n_3} F_A(hkl) e^{\pi i h p_{n_3}} e^{2\pi i(n_3 l)} . \quad (5)$$

In case $h = 2n$, $e^{\pi i h p_{n3}} = 1$, irrespective of the value p_{n3} and $F_C(\mathrm{hkl}) = N_1 N_2 N_3 F_A(hkl)$ as for an ordered crystal.

In case $h = 2n + 1$, $e^{\pi i h p_{n3}} = \cos \pi h p_{n3} = S_{n3} = 1$ or -1 for $p_{n3} = 0$ and 1, respectively, so that we can write for the *h* = *odd* reflections:

$$\begin{aligned} F_C(hkl) &= N_1 N_2 \sum_{n_3} F_A(hkl) S_{n_3} e^{2\pi i(n_3 l)} \\ &= N_1 N_2 F_A(hkl) \sum_{n_3} S_{n_3} e^{2\pi i(n_3 l)} \end{aligned} \quad (6)$$

so it is merely the product of the structure factor $F_A(hkl)$ and a lattice summation in *l* over the S_{n3} values. We performed simulations of the last part of Equation (6), by generating distributions of S_{n3} or by using correlation coefficients that describe the stacking probability.

Model 1

The first approach is to generate a random sequence of *A* and *B* double layers, which is equivalent to selecting random values of S_{n3}, either –1 or 1. We used a maximum value for n_3 = 40 for the crystal size (assuming that no correlations longer than 40 layers occur; this is obviously the case for a random arrangement) and repeated the simulation 2000 times adding the resulting structure factors $F_c(hkl)$ incoherently, i.e. the intensity

$$I(hkl) = \sum_{2000} F_c(hkl).F_c^*(hkl) .$$

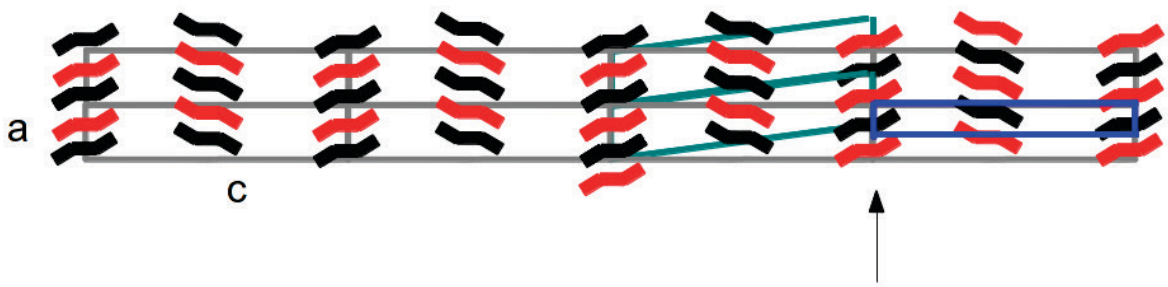

Figure 8. Schematic view of the CuSal structure down the **b** axis. Orthorhombic unit cell is indicated by grey lines. Layers consist of black and red complexes along **a**, that are oriented in up and down directions along **b**, respectively, as seen in Figure 6. A stacking fault of $\frac{1}{2}$**a** is indicated by the arrow, and the molecules pack into the monoclinic lattice, indicated by green lines. The stacking lattice on which all black complexes scatter in phase is indicated by blue lines.

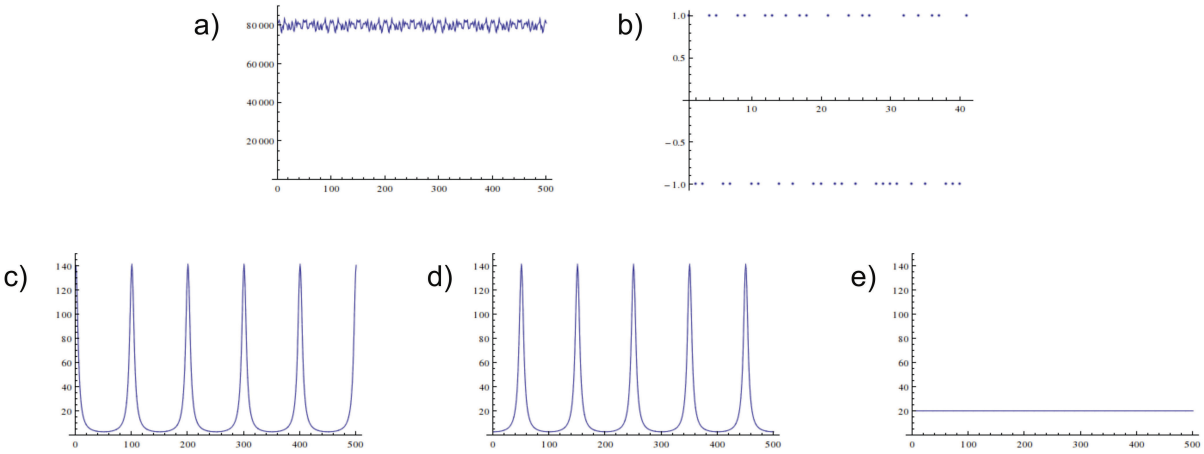

Figure 9. Simulations of the lattice function of Equation (6) for *l* ranging from 0–5. Model 1: a) Resulting lattice sum as function of *l* (× 100). b) Random sequence of signs S_{n3} for one crystal of n_3 = 40. Model 2: Lattice sums as function of *l* for the Markov chains: c) Low probability of stacking fault α = 0.1, C_1 = 0.8, d) larger probability of stacking faults α = 0.9, C_1 = –0.8 and e) no preferred nearest neighbour interaction α = 0.5, C_1 = 0. Only random stacking of double-layers produces rods in reciprocal space.

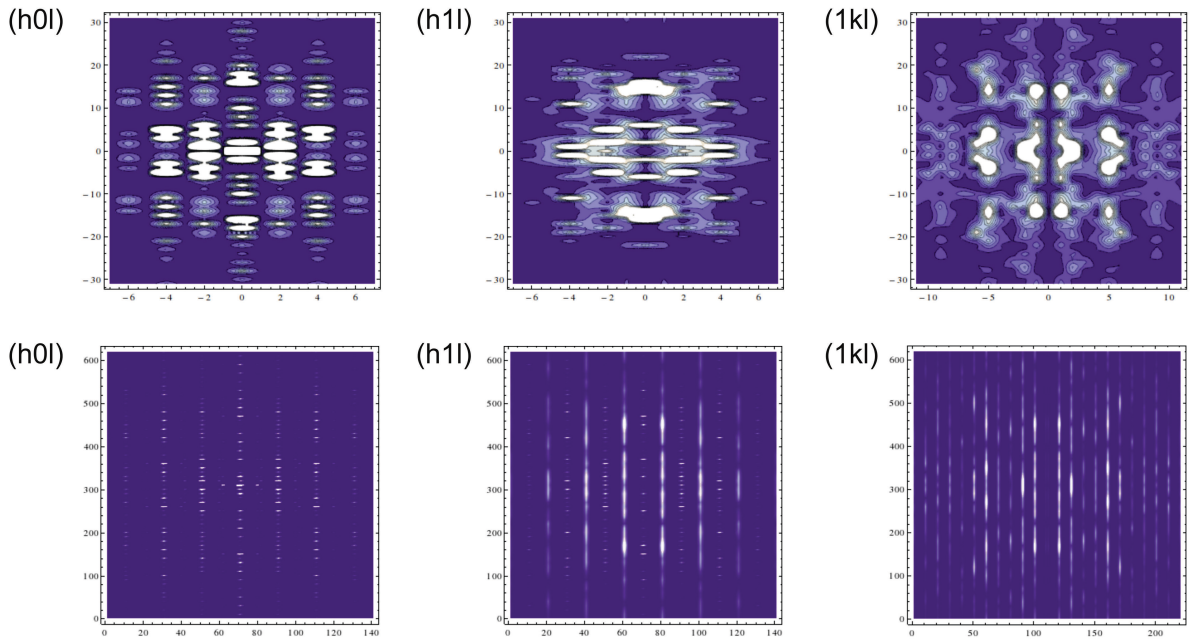

Figure 10. Sections through reciprocal space. Top: unit cell F^2_{calc} of the orthorhombic structure. Bottom: after multiplication with the lattice function.

Model 2

The correlation of layer stacking can be written in a way similar to Ref. [20] The scattered intensity is

$$F_c(hkl)F_c^*(hkl) = N_1^2N_2^2\sum_{n_3}\sum_{n_{3'}}F_A(hkl)F_A^*(hkl)e^{\pi ih(p_{n_3}-p_{n_{3'}})}e^{2\pi i((n_3-n_{3'})l)}$$
$$= N_1^2N_2^2\sum_{n_3}\sum_{n_{3'}}F_A(hkl)F_A^*(hkl)S_{n_3}S_{n_{3'}}e^{2\pi i((n_3-n_{3'})l)} \quad (7)$$

For *h* = *even* all S_{n3} and $S_{n3'}$ are equal to 1, and for *h* = *odd* Equation (6) can be written as

$$= N_1^2N_2^2F_A(hkl)F_A^*(hkl)\left[\sum_{n=1}^{N_3}2(N_3-n)C_n\cos(2\pi nl)+N_3\right] \quad (8)$$

where the sign function $S_{n3}S_{n3'}$ is represented by a correlation coefficient C_n, and $n = n_3 - n_{3'}$. This model for introducing correlation is the so-called Markov chain. Only nearest-neighbour interactions between layers are

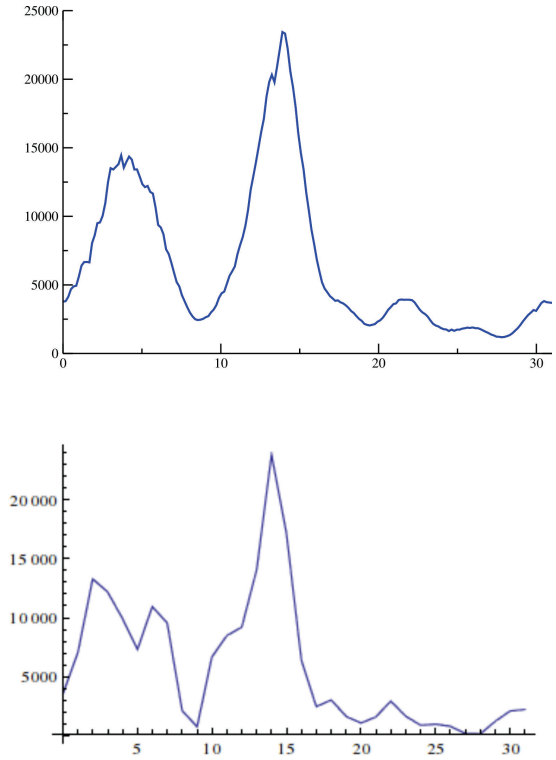

Figure 11. Profile of the 11*l* direction. The *l* index is shown on the abscissa. The ordinate shows the intensities on an arbitrary scale. Top: Experimental data from a 3-dimensional reconstruction using the program `img2hkl` of the Eval15 suite.[10] Some instrumental broadening from the diffraction experiment is clearly present. Bottom: Simulation results.

significant and the probability that layer *A* is stacked on the previous layer is given by $\alpha + C_1$ or α, for the previous layer being *A* and *B*, respectively. α is the probability of a stacking fault and C_1 is the nearest neighbour correlation. Subsequent layers have correlation coefficients $C_n = C_1^n$ as shown by Welberry.[20]

Results from the Diffuse Scattering

The lattice sum of Equation (6), for randomly stacked double-layers (Model 1) for $h = 2n + 1$ is a nearly constant function in *l* (Figure 9a). A typical example of the S_{n3} values in a crystallite of 40 unit cells is also shown (Figure 9b). The Markov chain model (Model 2) only gives a constant lattice sum in *l* for $C_1 = 0$, i.e. no correlation between neighbouring layers; positive C_1 gives maxima at Bragg positions and negative C_1 maxima in between those (Figure 9c–e). Thus the diffuse streaks in **c*** without Bragg spots are only explained when no correlation between stacked layers (*A* or *B*) exists.

The rods we observe in Figure 1 do not show any Bragg peaks, but also do not have constant intensity. This modulation in intensity[4] is caused by the structure factor $F_A(hkl)$ as seen in Equation (6). This can be shown by calculating the continuous unit cell Fourier transform $F_A(hkl)$ from the refined orthorhombic structure and then multiplying these with the lattice functions of the ordered lattice ($h = 2n$, k, l) or the rods ($h = 2n + 1$, k, l). The reconstruction of the experimental data with the program `precession` (Figure 1) delivers apparent non-integer values due to instrumental broadening. To mimic this in our model calculations, a widened lattice function was applied. The resemblance of the experimental data in Figure 1 with the simulation in Figure 10 is overall very good. As an example, we show the profile along the diffuse 11*l* direction in Figure 11.

CONCLUSIONS

We re-determined the crystal structure of CuSal, $Cu(C_7H_5O_3)_2(H_2O)_2$, in both the orthorhombic (MDO_1) and monoclinic phases (MDO_2). The structure is characterized by one-dimensional coordination polymers in **b** direction which are linked by hydrogen bonds into two-dimensional sheets in the **ab** plane. The crystal diffracts with diffuse streaks along **c*** for all *h* = *odd*, which are caused by packing faults of ordered two-dimensional **ab**-layers shifted over $\frac{1}{2}$**a**, which converts one phases to the other. The MDO_1 and MDO_2 lattices overlap every second period along **c** such that all reflections with *h* = *even* are from a ordered structure, be it orthorhombic or monoclinic. Both structures could be solved with *h* = *even* reflections only and the hydrogen bonding scheme could be unambiguously established. Diffuse streaks could be explained by a Markow chain growth model similar to Ref. [4]. In contrast to their crystals, our crystal shows complete absence of Bragg reflections on the diffuse streaks, implying random stacking of **ab**-layers, as we show by lattice sum simulations. Intensity modulation on the diffuse streaks is completely explained by the underlying unit cell Fourier transform of the orthorhombic description. As a consequence of the $\frac{1}{2}$**a** shift, which converts one phase to the other, it is irrelevant from which MDO structure we derive our description.

EXPERIMENTAL

Crystallization

Green crystals of the title compound were obtained in the same crystallization experiment as the brown crystals of Ref. [6].

X-ray Crystal Structure Determination

A green crystal of approximately 0.06 × 0.18 × 0.43 mm^3 was mounted on a Bruker Kappa ApexII diffractometer with sealed tube and Triumph monochromator (λ = 0.71073 Å) at a temperature of 105(2) K. 13 ϕ and ω scans were performed with a rotation increment of 0.3 °, a detector distance of 60 mm, and an exposure time of 10 s/frame. Intensity data were integrated with the Eval15 software[10] up to a resolution of $(\sin\theta/\lambda)_{max}$ = 0.70 Å^{-1}. Two integration runs were performed, one with a single orthorhombic lattice (i.e. reciprocal axes matrix) and one with a single monoclinic lattice (i.e. reciprocal axes matrix). The prediction of reflection profiles was based on an isotropic mosaicity of 0.3 ° and a *mica* contribution of 0.5 along *c**. Absorption correction and scaling of the integrated data was performed with SADABS.[21] This data reduction resulted in two datasets with orthorhombic and monoclinic symmetry, respectively.

Before the structure refinement, the datasets were "de-twinned": the orthorhombic dataset was deprived from the monoclinic contribution and *vice versa*. Reflections with *h* = *even* were considered as orthorhombic/monoclinic overlaps, and reflections with *h* = *odd* as non-overlapping. The "de-twinning" was based on calculated structure factors. Reflections with negative intensity were not "de-twinned" but omitted. For the calculation of the monoclinic F^2_{calc} a rotation twin about *c** was assumed with a twin fraction of 50 %. The calculation of the orthorhombic F^2_{calc} was based on a 50 % inversion twin. In the case of the orthorhombic dataset, the F^2_{calc} were scaled with *FVAR* = 0.21 for the orthorhombic, and *FVAR* = 0.18 for the monoclinic contribution. For the monoclinic dataset, the corresponding scale factors were *FVAR* = 0.21 for the monoclinic, and *FVAR* = 0.17 for the orthorhombic contribution. This slight inconsistency in scale factors is probably a consequence of the diffuse intensities in the *h* = *odd* layers.

Coordinates for the starting models were taken from Ref. [2]. The orientational disorder of the salicylate molecules could not be reproduced and we refined ordered salicylate ligands with the hydroxy group on only one of the *ortho* positions on the aromatic ring.

Table 3. Experimental details for the orthorhombic setting. Refined as an inversion twin. Contributions of the monoclinic structure removed from the structure factors

Molecular formula	$Cu(C_7H_5O_3)_2(H_2O)_2$	
Formula weight	373.79	
Crystal system	Orthorhombic	
Space group	$Pca2_1$	
a / Å	7.65385(11)	
b / Å	11.7378(3)	
c / Å	31.5707(6)	
V / Å^3	2836.28(9)	
Z	8	
D_x / g cm^{-3}	1.751	
μ / mm^{-1}	1.58	
refl. condition	*h* = *even*, *odd*	*h* = *even*
No. of meas. refl.	82594	41161
No. of unique refl.	8286	4342
R_{int}	0.0500	0.0378
Completeness	99.9 %	52.9 %
No. of parameters	420	420
No. of restraints	791	791
Twin fraction (BASF)	0.46(3)	0.50(4)
R1/wR2 (obs.)	0.0564 / 0.1589	0.0371 / 0.0958
R1/wR2 (all refl.)	0.0578 / 0.1609	0.0392 / 0.0983
Goodness of Fit	1.135	1.146
$\Delta\rho_{max}$ / e Å^{-3}	2.32	0.44
$\Delta\rho_{min}$ / e Å^{-3}	–2.66	–0.53

Table 4. Experimental details for the monoclinic setting. Refined as a rotation twin. Contributions of the orthorhombic structure removed from the structure factors.

Molecular formula	$Cu(C_7H_5O_3)_2(H_2O)_2$	
Formula weight	373.79	
Crystal system	Monoclinic	
Space group	$P2_1/a$	
a / Å	7.6558(2)	
b / Å	11.7408(3)	
c / Å	31.8085(12)	
β / °	96.931(2)	
V / Å^3	2838.22(15)	
Z	8	
D_x / g cm^{-3}	1.750	
μ / mm^{-1}	1.58	
refl. condition	*h* = *even*, *odd*	*h* = *even*
No. of meas. refl.	86764	43435
No. of unique refl.	8262	4322
R_{int}	0.0508	0.0390
Completeness	99.7%	52.2%
No. of parameters	420	420
No. of restraints	774	774
Twin fraction (BASF)	0.4627(18)	0.501(6)
R1/wR2 (obs.)	0.0650 / 0.1845	0.0431 / 0.1107
R1/wR2 (all refl.)	0.0678 / 0.1876	0.0473 / 0.1132
Goodness of Fit	1.064	1.212
$\Delta\rho_{max}$ / e Å^{-3}	3.21	0.40
$\Delta\rho_{min}$ / e Å^{-3}	–2.02	–0.55

Least-squares refinement was performed with SHELXL-2018.[22] A rather large number of restraints was used in the refinement concerning the geometric equivalence between the salicylate ligands and their flatness (instructions *SAME* and *FLAT*). Non-hydrogen atoms were refined with anisotropic displacement parameters and restrained using *ISOR* and *RIGU* instructions. Hydrogen atoms of the water molecules were kept fixed on their positions from difference-Fourier maps. All other hydrogen atoms were refined with a riding model. The orthorhombic structure was refined as inversion twin. For the monoclinic structure refinement we used a twin matrix of (–1,0,0/0,–1,0/1,0,1) which corresponds to a twofold rotation about *hkl* = (0,0,1) or *uvw* = [–1,0,–2].

Summaries of the structural details are given in Table 3 and Table 4. The Tables give the results for refinements on all data and on data with *h* = *even* only. Figures of the molecular structures were prepared with the programs PLATON[16] and ToposPro.[23] CCDC 1841406-1841408 and 1850913 contain the supplementary crystallographic data for this paper. These data can be obtained free of charge from The Cambridge Crystallographic Data Centre via www.ccdc.cam.ac.uk/data_request/cif.

Simulations

Simulations of lattice sum of Equation (7) are carried out with Mathematica.[24] The summation is over 40 unit cells in the **c** direction (n_3 = 40) and repeated 2000 times. The structure factor $F_A(hkl)$ is set to 1.0, and also $N_1 = N_2 = 1$. For model 1, random values of –1 or 1 were generated for p_{n3} using the `RandomInteger` function in Mathematica. For model 2, Equation (8) was calculated, while setting $N_1 = N_2 = 1$ and $F_A = F_A^* = 1$. C_1 is the nearest neighbour correlation and α is the probability of a stacking fault. The two parameters are related through $\alpha = m_A(1-C_1)$, where m_A is the fraction of layers A in the crystal, which we assume to be 0.5. The probability of stacking the same layers (A on A and B on B) is $\alpha + C_1$, while that of stacking different layers (A on B or B on A) is α. Inclusion of values for $F_A(hkl)$ in Equation (6) leads to modulation of the diffuse scattering on the rods with $h = 2n + 1$. F_A^2 values were calculated from the coordinates of the orthorhombic structure (setting B = 2.0 Å^2) at integer values of *hkl*; intermediate values are obtained through interpolation with Mathematica `Interpolation` (Figure 10 (top)). As the simulations have shown that only Bragg spots or diffuse lines occur, we represented the lattice sums of Equation (6) by a lattice function having sharp maxima at Bragg positions and rods for the diffuse layer lines; these are multiplied with F_A^2 to get the images in Figure 10 (bottom).

REFERENCES

[1] K. Dornberger-Schiff, T. I. Malinowski, *Acta Crystallogr.* **1966**, *21*, A171.

[2] S. Jagner, R. G. Hazell, K. P. Larsen, *Acta Crystallogr., Sect. B: Struct. Crystallogr. Cryst. Chem.* **1976**, *32*, 548.

[3] S. Tjotta, E. J. Samuelsen, S. Jagner, *J. Phys.: Condens. Matter* **1991**, *3*(*20*), 3411.

[4] E. J. Samuelsen, S. Tjotta, S. Jagner, *J. Phys.: Condens. Matter* **1991**, *3*(*20*), 3421.

[5] E. J. Samuelsen, S. Jagner, *Phase Transitions* **1993**, *43*(*1–4*), 89.

[6] J. A. v. d. Horn, M. Lutz, *Acta Crystallogr., Sect. E: Struct. Rep. Online* 2017, 73, 235.

[7] G. Ferraris, E. Makovicky, and S. Merlino, *Crystallography of Modular Materials*, vol. 15 of *IUCr Monographs of Crystallography*, ch. 2, pp. 127–206. Oxford University Press, **2004**.

[8] S. Ďurovič, J. Hybler, *Z. Kristallogr. - Cryst. Mater.* **2006**, *221*(*1*), 63.

[9] B. Stöger, *Symmetry* **2014**, *6*(*3*), 589.

[10] A. M. M. Schreurs, X. Xian, L. M. J. Kroon-Batenburg, *J. Appl. Crystallogr.* **2010**, *43*, 70.

[11] T. L. Falch, J. B. Fløystad, D. W. Breiby, A. C. Elster, *IEEE Access* **2013**, *1*, 564.

[12] J. A. van der Horn, B. Souvignier, M. Lutz, *Crystals* **2017**, *7*(*12*), 377.

[13] A. W. Addison, T. N. Rao, J. Reedijk, J. van Rijn, G. C. Verschoor, *J. Chem. Soc., Dalton Trans.* **1984**, 1349.

[14] M. Lutz, A. L. Spek, *Acta Crystallogr., Sect. C: Cryst. Struct. Commun.* **2009**, *65*, m69.

[15] H. D. Flack, *Acta Crystallogr., Sect. A: Found. Crystallogr.* **1983**, *39*, 876.

[16] A. L. Spek, *Acta Crystallogr., Sect. D: Biol. Crystallogr.* **2009**, *65*, 148.

[17] B. T. M. Willis, *Proc. R. Soc. Lond. A* **1958**, *248*(*1253*), 183.

[18] W. A. Wooster, *Diffuse X-Ray reflections from crystals*. New York: Dover, **1997**.

[19] K. Dornberger-Schiff, *Acta Crystallogr.* **1956**, *9*, 593.

[20] T. R. Welberry, *Diffuse X-ray Scattering and Models of Disorder*, vol. 16 of *IUCr Monographs on Crystallography*. Oxford University Press, **2004**.

[21] L. Krause, R. Herbst-Irmer, G. M. Sheldrick, D. Stalke, *J. Appl. Crystallogr.* **2015**, *48*, 3.

[22] G. M. Sheldrick, *Acta Crystallogr., Sect. C: Struct. Chem.* **2015**, *71*, 3.

[23] V. A. Blatov, A. P. Shevchenko, D. M. Proserpio, *Cryst. Growth Des.* **2014**, *14*(*7*), 3576.

[24] Wolfram Research Inc., *Mathematica 9.0*, **2012**.